1-1-2017

Platinum-Cobalt Bimetallic Nanoparticles with Pt Skin for Electro-Oxidation of Ethanol

Binwei Zhang
University of Wollongong, Xiamen University, bz370@uowmail.edu.au

Tian Sheng
Xiamen University

Yunxiao Wang
University of Wollongong, yunxiao@uow.edu.au

Xi-Ming Qu
Xiamen University

Jun-Ming Zhang
Xiamen University

See next page for additional authors

Platinum-Cobalt Bimetallic Nanoparticles with Pt Skin for Electro-Oxidation of Ethanol

Abstract

In order to maximize the Pt utilization in catalysts and improve catalytic processes, we report a convenient strategy for preparation of Pt3Co with Pt-skin structured bimetallic nanocatalysts directly supported on porous graphitic carbon. Notably, the thickness of the Pt-skin is only 1-2 atomic layers, about 0.5 nm. Surprisingly, the bimetallic nanocatalysts composed of Pt3Co with Pt-skin are first used as ethanol electro-catalysts, with the mass activity of 0.79 mA ¿gPt-1, which is a 250% enhancement compared with commercial Pt/C (0.32 mA ¿gPt-1). On the basis of the results of electrochemical in situ Fourier transform infrared spectroscopy (FTIRS) and density functional theory (DFT), a new ethanol electro-oxidation enhancement mechanism is proposed in which Pt3Co with Pt-skin promotes partial oxidation of ethanol over C-C bond cleavage, thereby resulting in higher CH3COOH production than CO2 production.

Keywords

ethanol, bimetallic, electro-oxidation, nanoparticles, skin, pt, platinum-cobalt

Disciplines

Engineering | Physical Sciences and Mathematics

Publication Details

Zhang, B., Sheng, T., Wang, Y., Qu, X., Zhang, J., Zhang, Z., Liao, H., Zhu, F., Dou, S., Jiang, Y. & Sun, S. (2017). Platinum-Cobalt Bimetallic Nanoparticles with Pt Skin for Electro-Oxidation of Ethanol. ACS Catalysis, 7 (1), 892-895.

Authors

Binwei Zhang, Tian Sheng, Yunxiao Wang, Xi-Ming Qu, Jun-Ming Zhang, Zong-Cheng Zhang, Hong-Gang Liao, Fu-Chun Zhu, Shi Xue Dou, Yan-Xia Jiang, and Shi-Gang Sun

Platinum–Cobalt bimetallic nanoparticles with Pt skin for electro-oxidation of ethanol

Bin-Wei Zhang[a,b], Tian Sheng[a], Yun-Xiao Wang[b], Xi-Ming Qu[a], Jun-Ming Zhang[a], Zong-Cheng Zhang[a], Hong-Gang Liao[a], Fu-Chun Zhu[a],Shi-Xue Dou[b], Yan-Xia Jiang[a,*] and Shi-Gang Sun[a,*]

[a,] State Key Laboratory of Physical Chemistry of Solid Surfaces, Department of Chemistry, College of Chemistry and Chemical Engineering, Xiamen University, Xiamen 361005, China

[b,] Institute for Superconducting and Electronic Materials, Australian Institute of Innovative Materials, University of Wollongong, Innovation Campus, Squires Way, North Wollongong, New South Wales 2500, Australia.

Supporting Information Placeholder

ABSTRACT: In order to maximize the Pt utilization in catalysts and improve catalytic processes, we report a convenient strategy for preparation Pt_3Co with Pt-skin structured bimetallic nanocatalysts directly supported on porous graphitic carbon. Notably, the thickness of the Pt-skin is only 1–2 atomic layers, about 0.5 nm. Surprisingly, the bimetallic nanocatalysts composed of Pt_3Co with Pt-skin are firstly used as ethanol electro-catalysts, with the mass activity of 0.79 mA μgPt^{-1}, which is 250% enhancement compared with commercial Pt/C (0.32 mA μgPt^{-1}). Based on the results of electrochemical *in-situ* Fourier transform infrared spectroscopy (FTIR) and density functional theory (DFT), a new ethanol electro-oxidation enhancement mechanism is proposed in which Pt_3Co with Pt-skin promotes partial oxidation of ethanol over C-C bond cleavage, thereby resulting in higher CH_3COOH production than CO_2 production.

Bimetallic nanoparticles play a vital role in energy conversion and storage, for instance supercapacitor, battery, fuel cell, and solar fuel [1]. Unlike monometallic nanoparticles, bimetallic nanoparticles ordinarily show better than the sum of its parts since them could create synergistic effect during them combination [2]. It is worth mentioning that electro-catalytic reactions only happen on electro-catalysts surface[3]. It is significant to investigate the surface composition of bimetallic catalysts thus a deeper understanding of electro-catalytic reaction mechanism, kinetics and energy efficiency would be produced.

Platinum equips with the attribute of excellent efficiency in electrocatalyst for ethanol electro-oxidation. Nevertheless, it is difficult to widely apply Pt in direct ethanol fuel cells (DEFCs) for both stationary and portable applications, since the barriers of the prices and scarcity of Pt. It is widely acknowledged that CH_3CH_2OH electro-oxidation involves two parallel pathways, the complete oxidation ($CH_3CH_2OH + 3H_2O = 2CO_2 + 12H^+ + 12e$) and the incomplete oxidation ($CH_3CH_2OH + H_2O = CH_3COOH + 4H^+ + 4e$). In addition, Pt catalyst is inefficient at breaking the C-C bond in ethanol oxidation. Considerable progress has been made towards improving ethanol electro-oxidation performance on Pt-based bimetallic electrocatalysts, such as alloying with Pd [4], SnO_2 [5], and Rh [6]. Meanwhile, atomic steps, ledges, and kinks were proven to play a significant role in ethanol electro-oxidation in our previous work [7]. And the Pt_3Ni catalysts show different catalytic activity in terms of oxygen reduction reaction when the surface is tuned from Pt-skin to Ni-rich surface [8]. Since the atomic steps, ledges, and kinks of Pt-skin catalysts are different from those of pure Pt catalysts, we synthesized Pt_3Co with a Pt-skin surface, supported on porous graphitic carbon (PC) (denoted as Pt_3Co@Pt/PC). Pt and Co precursors were reduced by controlled thermal treatment, and the Pt_3Co nanoparticles were well-dispersed on PC, even after high temperature treatment (see Supporting Information). The reason of formation of Pt-skin may be following this: firstly, at 300 °C during 3 h, platinum and cobalt precursors are reduced at forming gas (10 vol % H_2 in nitrogen), at this process platinum and cobalt precursors have been reduced. This process facilitates a surface segregation of Pt because it has a trend to form moderate segregation[8]. Further, while it was heated up to 700 °C for 3 h, the segregation of Pt happened on the surface and the high temperature provides H_2 enough energy to preferentially combine with Pt on the surface[3a], which process is like high temperature process to form Pt-skin on single crystal[3c]. This study is the first exploration of ethanol electro-oxidation on Pt-skin of Pt_3Co/PC, and it exhibited superior activity. Atomic resolution high-angle annular dark field (HAADF) scanning transmission electron microscope (STEM) imaging, coupled with electrochemical *in-situ* FTIR spectroscopy, are used to confirm the thickness of the Pt-skin is 1–2 atomic layers, about 0.5 nm. *In-situ* FTIR and DFT give a new insight into breakage of the C-C bonds in ethanol on Pt_3Co@Pt/PC and Pt/C. In contrast to Pt/C, the Pt-skin of Pt_3Co@Pt/PC is easier to produce acetic acid for ethanol electro-oxidation.

Figure 1a presents the atomic-resolution annular dark-field (ADF)-STEM image of Pt_3Co@Pt/PC. It should be pointed out that the relationship between image's pixel intensity and the element number Z is the proportion on the whole in the HAADF imaging mode [9], so compared with the Co columns, the Pt columns would show higher intensity, thus leading to higher Pt intensity than that of Pt_3Co [8]. Therefore, we examined four sites of Pt_3Co@Pt/PC. The intensities of the four sites in Pt_3Co@Pt/PC were determined by intensity analysis, which are shown in Figure 1b-e, respectively. Both sites L1 and L3 have 2 Pt atomic layers; sites L2 and L4 have 1 Pt atomic layer. As shown in the Figure 1f of the high-resolution TEM (HRTEM), the *d*-spacing of the edge is measured to be 2.27 Å, which is consistent with Pt (111) [10], and the *d*-spacing of the center is ~ 2.22 Å, which could correspond to Pt_3Co(111) [11]. It indicates that the Pt_3Co@Pt/PC is Pt-skin surface; the center is Pt_3Co alloy. An ADF-STEM image of a nanoparticle

is showed in figure 2a, which is spectroscopically imaged. The Pt element and Co element projected distributions in this particle in figure 2b-c. The composite image of Pt versus Co (Figure 2d) suggested that the surface of this nanoparticle contains more amount of Pt than Co. Furthermore, Figure 2e presents the corresponding line-profile analysis from figure 2d shown by the arrow, which confirms that the thickness of Pt-skin is ~0.5 nm, corresponding to 2 atomic layers, consisting with the ADF results.

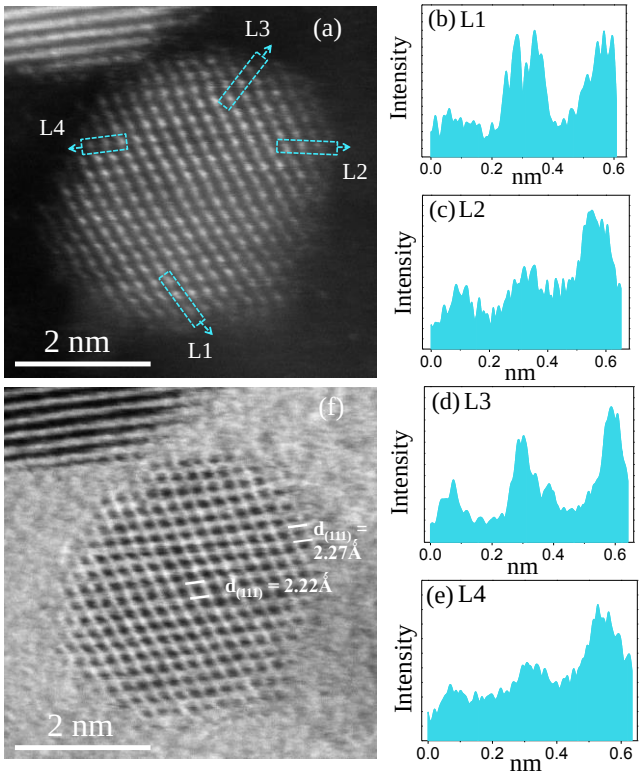

Figure 1(a) Atomic-resolution ADF-STEM image of Pt_3Co@Pt/PC, with the intensity of sites L1, L2, L3, and L4 shown in (b)–(e); (f) HRTEM image of Pt_3Co@Pt/PC.

The TEM image of Pt_3Co@Pt/PC (Figure S2a in the Supporting Information) clearly shows that the Pt_3Co@Pt nanoparticles are well dispersed with a high loading on PC. The average diameter of Pt_3Co@Pt nanoparticles (Figure S2b) is evaluated to be 3.06 ± 0.86 nm from 200 nanoparticles. The X-ray diffraction (XRD) of Pt_3Co@Pt/PC and Pt/C (Johnson Matthey) are shown in figure S3. The broad peaks near 25º of two catalysts are assigned to carbon; peaks at 40.3º, 46.8º, 68.2º, 82.7º of Pt_3Co@Pt/PC are agreement with that of Pt/C, which present Pt face-centered cubic (fcc) features. Compared to Pt/C, all broad diffraction peaks of Pt_3Co@Pt/PC are at high angles, because Co atoms are incorporated into the Pt fcc structure, forming Pt_3Co alloy [12].

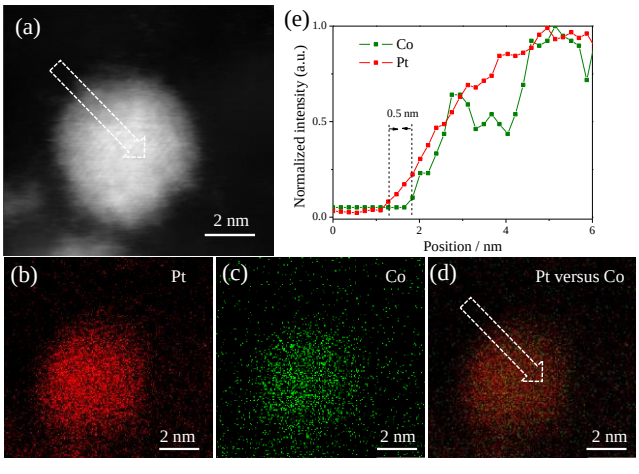

Figure 2(a) ADF-STEM image of Pt_3Co@Pt/PC nanoparticle. (b-d) 2D electron energy loss spectroscopic mapping of Pt (red), Co (green), and the composite image of Pt *vs* Co. (e) Line-profile analysis from the indicated area of (a) and (d), demonstrating about 0.5 nm Pt skin thickness.

Cyclic voltammograms (CVs) of Pt_3Co@Pt/PC and Pt/C are shown in Figure S4a, where the Pt/C exhibits the well-known hydrogen adsorption and desorption of pure Pt nanoparticles dispersed on carbon black in 0.1 M $HClO_4$ solution. In contrast, the CV of Pt_3Co@Pt/PC does not show any apparent hydrogen adsorption and desorption, which is probably because the presence of Co in the Pt_3Co@Pt/PC results in reduced hydrogen adsorption and desorption capacity. CO_{ad} stripping curves of two catalysts are shown in Figure S4b. The ratio of integrated charges (Q_{CO} / $2Q_H$) between CO stripping (Q_{CO}) and under potential deposition of hydrogen H_{upd} (Q_H) is calculated to be 1.54 and 1.10 for Pt@Pt_3Co/PC and Pt/C, respectively, in table S2. This relationship is in good agreement with the Pt-skin structure [13].

On pure Pt, electro-oxidation of formic acid would form poisoning intermediates (CO_{ad}) via "dual pathway" because the CO poisoning takes place on at least two consecutive Pt surface sites [14]. For Pt_3Co@Pt/PC, the surface is Pt; so HCOOH may form adsorbed CO (CO_{ad}) through the dual pathway mechanism on Pt_3Co@Pt/PC [8]. Figure S5a shows the CVs of Pt/C and Pt_3Co@Pt/PC in 0.1 M HCOOH + 0.1 M $HClO_4$ solution. The Pt_3Co@Pt/PC oxidation of HCOOH is similar to that of Pt/C, which also has two anodic peaks. This suggests that both Pt_3Co/PC (Pt-skin) and Pt/C operate via the dual pathway mechanism poisoned by CO_{ad}. Electrochemical *in-situ* FTIR spectra of HCOOH oxidation are shown in Figure S5b and S5c. Reference spectrum potentials are collected at -0.25 V, and working spectrum potentials vary from -0.20 to 0.70 V (0.1 V interval). The band at 2345 cm^{-1} is a characteristic peak of CO_2 asymmetric stretching vibration that originates from direct HCOOH oxidized and CO_{ad} oxidized, which can be observed in both catalysts. The band at 2050 cm^{-1} corresponds to linearly bonded CO (CO_L), which goes through the poisoning route. It is noteworthy that CO_L could be found clearly for both Pt_3Co@Pt/PC and Pt/C, which indicates that oxidation of HCOOH via the poisoning route on Pt_3Co@Pt/PC as well. This conclusion furtherly implies that Pt_3Co@Pt/PC has a Pt-skin [8]. Moreover, the activity of Pt_3Co@Pt/PC is better than that of Pt/C; it attributes that the subsurface layers of Co atoms may affect the electronic structure of the outermost Pt-skin.

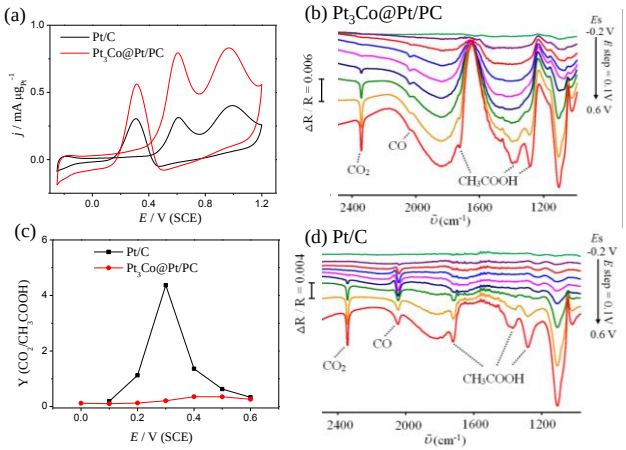

Figure 3(a) Cyclic voltammograms (CVs) of Pt_3Co@Pt/PC and Pt/C in 0.1 M CH_3CH_2OH + 0.1 M $HClO_4$ solution, 50 mV s^{-1}. *In-situ* mass spectroscopy (MS) FTIR spectra of (b)

Pt_3Co@Pt/PC and (d) Pt/C for CH_3CH_2OH oxidation in 0.1 M CH_3CH_2OH + 0.1 M $HClO_4$. (c) Ratio of integrated intensities of CO_2 and intensities CH_3COOH as a function of working potentials of the two electrocatalysts.

Electrocatalytic oxidation of ethanol in acidic solution (0.1 M $HClO_4$ + 0.1 M CH_3CH_2OH) was used to study the catalytic property of the Pt_3Co@Pt/PC, as shown in Figure 3a. It is obvious that Pt_3Co@Pt/PC and Pt/C show similar CV curves, which display two peaks at 0.60 V and 0.96 V, corresponding to the well-known ethanol electro-oxidation [6b]. The first peak (at 0.60 V) is ascribed to formation of CH_3CHO, CH_3COOH and CO_2; the following peak ~ 0.96 V is assigned to CH_3COOH. Significantly, the current density of Pt_3Co@Pt/PC is 0.79 mA μg_{Pt}^{-1} at 0.60 V, which is 2.5 times as high as that of Pt/C (0.32 mA μg_{Pt}^{-1}). Figure S6 shows the current-time cures at 0.45 V on Pt_3Co@Pt/PC and Pt/C at room temperature. After 3600 s, the activity of Pt_3Co@Pt/PC is still better than that of Pt/C, regardless of its mass activity or specific activity.

To understand the impact of the Pt-skin surface of Pt_3Co@Pt/PC electro-catalyst on ethanol, *in-situ* FTIR contributes to recognize the intermediate and final products to identify the selectivity towards CH_3CH_2OH electro-oxidation, as shown in Figure 3b (Pt_3Co@Pt/PC) and 3d (Pt/C). The signature peak of CO_2 (~2345 cm^{-1}) corresponds to complete oxidation of CH_3CH_2OH, which represents the breaking of the C-C bond in CH_3CH_2OH oxidation. The band at ~1720 cm^{-1} is attributed to the C=O bond's stretching vibration in CH_3CHO and CH_3COOH, which indicates incomplete electro-oxidation of CH_3CH_2OH. The characteristic absorption band of C-O stretching in CH_3COOH at 1280 cm^{-1} is typically applied to quantitative analysis of CH_3COOH. Remarkably, lines for bound CO (CO_L) at 2050 cm^{-1} could be found in both the Pt/C and the Pt_3Co@Pt/PC catalysts, which furtherly indicate that Pt_3Co@Pt/PC possesses a Pt skin. Figure S7 shows the variation of the integrated intensities of the 2345 cm^{-1} band (CO_2) and the 1280 cm^{-1} band (C-O) corresponding to potential for Pt_3Co/PC (Pt-skin) and commercial Pt/C samples. To investigate the capability for C-C bond breaking in CH_3CH_2OH, we plot the ratio of integrated intensities (I) associated with CO_2 (total electo-oxidation) and CH_3COOH (partial electro-oxidation) as a function of working potentials (Figure 3c). It can be clearly seen that the ratio of I_{CO_2}/I_{CH_3COOH} firstly raises but reduces subsequently when the applied potentials increases. Compared with Pt/C, the value of I_{CO_2}/I_{CH_3COOH} for Pt_3Co@Pt/PC is low, which suggests that the main product of Pt_3Co@Pt/PC is CH_3COOH. Pt is a poor catalyst for ethanol oxidation; adding Sn into Pt (PtSn) could ensemble electro-oxidize CH_3CH_2OH to CH_3COOH, which it is difficult to break the C-C bond[15]. When Sn is added on the surface of Pt, the alloy not only could minimize the poisoning effects but also improve the activity towards ethanol electro-oxidation[15a,16]. As for Sn, it could increase formation of OH species at lower potential, which could oxidize CH_3CHO to produce more CH_3COOH[15]. The comparison Pt_3Co@Pt/PC with Pt-Sn catalyst is listed in table S3. It could be found that specific activity of Pt_3Co@Pt/PC at 0.3 V is lower than PtSn[15b] and Pt_7Sn_3[17]. It may be attributed that the surface of Pt_3Co@Pt/PC is Pt-skin, however, the surface of PtSn[15b] and Pt_7Sn_3[17] have Sn, which help formation of OH species.

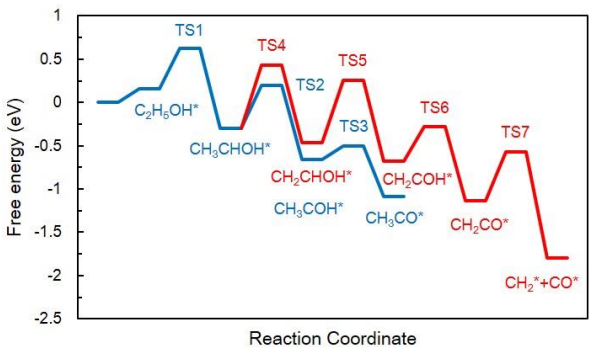

Figure 4 Energy profiles of ethanol electrooxidation on the stepped $Pt_3Co(211)$ surface.

The reaction mechanism of CH_3CH_2OH electro-oxidation on the stepped $Pt_3Co(211)$ surface with a Pt-skin structure were revealed by DFT calculations. The free energy is displayed in Figure 4 and all the calculated data and the optimized structures are shown in Figure S8 and S9. According to the previous theoretical investigation, CH_3CHOH^* can break the α-C-H bond or the β-C-H bond, and the barrier difference between them can be used to evaluate the CH_3COOH/CO_2 selectivity [18]. On stepped $Pt_3Co(211)$ surface, CH_3CHOH^* strongly prefers to break the α-C-H bond, producing CH_3COH^* with a barrier being 0.5 eV (transition state(TS) 2,) rather than breaking the β-C-H bond with a barrier being 0.73 eV (TS 4). Afterwards, CH_3CO^* readily forms after overcoming a barrier of 0.16 eV to break the O-H bond in CH_3COH^* (red line). CH_3CO^* is rather stable on the surface and would be oxidized to CH_3COOH^* at high potentials, leading the partial electro-oxidation of CH_3CH_2OH to CH_3COOH dominated, which is in consistent with the *in situ* FTIR observations. In the other way to break C-C bond starting from CH_2CHOH^*, the C-H bond breaking barrier is 0.72 eV to yield CH_2COH^*, and the O-H bond breaking barrier is 0.4 eV for the formation of CH_2CO^*. CH_2CO^* is a reasonable precursor to split the C-C bond to CH_2^* and CO^* with a low barrier of 0.57 eV (blue line).

In summary, the Pt_3Co@Pt/PC with the Pt-skin structure was successfully prepared by a sample controlled thermal treatment method. A unique Pt-skin structure is confirmed by a series of complementary techniques. The Pt-skin is 1-2 atomic layers with thickness of about 0.5 nm. Benefiting from the bimetallic synergetic effect and unique structural advantages, the mass activity of 0.79 mA μg_{Pt}^{-1} is achieved on Pt_3Co@Pt/PC, which is 2.5 times as high as that of Pt/C towards ethanol electro-oxidation. Via in-situ FTIR spectra and DFT, ethanol prefers to be broken α-C-H bond producing CH_3COH^* rather than breaking the β-C-H bond yielding CH_2COH^* on Pt_3Co@Pt/PC.

ASSOCIATED CONTENT

Supporting Information

Experimental details, related characterization, and supporting results and discussion. This material is available free of charge via the Internet at http://pubs.acs.org.

AUTHOR INFORMATION

Corresponding Author

yxjiang@xmu.edu.cn and sgsun@xmu.edu.cn

ACKNOWLEDGMENT

This work was supported by the National Natural Science Foundation of China (Grant Nos. 21273180, 21321062, 21361140374, 2015CB932303, 51421002, XDB07030200, 2014CB921002, and 51522212). The authors also acknowledge Dr.Tania Silver for her critical reading.

REFERENCES

[1] a) E. E. Benson, C. P. Kubiak, A. J. Sathrum, J. M. Smieja, *Chem Soc Rev* **2009**, *38*, 89-99; b) M. Sankar, N. Dimitratos, P. J. Miedziak, P. P. Wells, C. J. Kiely, G. J. Hutchings, *Chem Soc Rev* **2012**, *41*, 8099-8139; c) M. R. Gao, Y. F. Xu, J. Jiang, S. H. Yu, *Chem Soc Rev* **2013**, *42*, 2986-3017.

[2] a) D. Wang, Y. Yu, H. L. Xin, R. Hovden, P. Ercius, J. A. Mundy, H. Chen, J. H. Richard, D. A. Muller, F. J. DiSalvo, H. D. Abruña, *Nano Letters* **2012**, *12*, 5230-5238; b) C. Wang, N. M. Markovic, V. R. Stamenkovic, *ACS Catalysis* **2012**, *2*, 891-898.

[3] a) H. Liao, A. Fisher, Z. J. Xu, *Small* **2015**, *11*, 3221-3246; b) D. Volpe, E. Casado-Rivera, L. Alden, C. Lind, K. Hagerdon, C. Downie, C. Korzeniewski, F. J. DiSalvo, H. D. Abruña, *Journal of The Electrochemical Society* **2004**, *151*, A971; c) V. R. Stamenkovic, B. Fowler, B. S. Mun, G. F. Wang, P. N. Ross, C. A. Lucas, N. M. Markovic, *Science* **2007,** *315*, 493-497.

[4] a) C. Zhu, S. Guo, S. Dong, *Advanced Materials* **2012**, *24*, 2326-2331; b) K. Sasaki, H. Naohara, Y. Cai, Y. M. Choi, P. Liu, M. B. Vukmirovic, J. X. Wang, R. R. Adzic, *Angewandte Chemie, International Edition* **2010**, *49*, 8602-8607.

[5] W. Du, G. Yang, E. Wong, N. A. Deskins, A. I. Frenkel, D. Su, X. Teng, *J Am Chem Soc* **2014**, *136*, 10862-10865.

[6] a) A. Kowal, M. Li, M. Shao, K. Sasaki, M. B. Vukmirovic, J. Zhang, N. S. Marinkovic, P. Liu, A. I. Frenkel, R. R. Adzic, *Nature Materials* **2009**, *8* 325; b) L. Rao, Y.-X. Jiang, B.-W. Zhang, Y.-R. Cai, S.-G. Sun, *Physical Chemistry Chemical Physics* **2014**, *16*, 13662.

[7] N. Tian, Z.-Y. Zhou, S.-G. Sun, Y. Ding, Z. L. Wang, *Science* **2007**, *316*, 732-735.

[8] B.-W. Zhang, Z.-C. Zhang, H.-G. Liao, Y. Gong, L. Gu, X.-M. Qu, L.-X. You, S. Liu, L. Huang, X.-C. Tian, R. Huang, F.-C. Zhu, T. Liu, Y.-X. Jiang, Z.-Y. Zhou, S.-G. Sun, *Nano Energy* **2016**, *19*, 198-209.

[9] S. J. Pennycook, D. E. Jesson, *Ultramicroscopy* **1991**, *37*, 14-38.

[10] S.-I. Choi, S. Xie, M. Shao, J. H. Odell, N. Lu, H.-C. Peng, L. Protsailo, S. Guerrero, J. Park, X. Xia, J. Wang, M. J. Kim, Y. Xia, *Nano Letters* **2013**, *13*, 3420-3425.

[11] S. I. Choi, R. Choi, S. W. Han, J. T. Park, *Chemistry* **2011**, *17*, 12280-12284.

[12] D. Wang, H. L. Xin, R. Hovden, H. Wang, Y. Yu, D. A. Muller, F. J. DiSalvo, H. D. Abruña, *Nat Mater* **2013**, *12*, 81-87.

[13] a) D. F. van der Vliet, C. Wang, D. Li, A. P. Paulikas, J. Greeley, R. B. Rankin, D. Strmcnik, D. Tripkovic, N. M. Markovic, V. R. Stamenkovic, *Angewandte Chemie, International Edition* **2012**, *51*, 3139-3142; b) C. Chen, Y. J. Kang, Z. Y. Huo, Z. W. Zhu, W. Y. Huang, H. L. L. Xin, J. D. Snyder, D. G. Li, J. A. Herron, M. Mavrikakis, M. F. Chi, K. L. More, Y. D. Li, N. M. Markovic, G. A. Somorjai, P. D. Yang, V. R. Stamenkovic, *Science* **2014**, *343*, 1339-1343.

[14] a) S. Park, Y. Xie, M. J. Weaver, *Langmuir* **2002**, *18*, 5792-5798; b) E. Leiva, T. Iwasita, E. Herrero, J. M. Feliu, *Langmuir* **1997**, *13*, 6287-6293.

[15] a) Q. Wang, G. Q. Sun, L. H. Jiang, Q. Xin, S. G. Sun, Y. X. Jiang, S. P. Chen, Z. Jusys, R. J. Behm, *Physical chemistry chemical physics P* **2007,** *9*, 2686-2696; b) L. Rao, B.W. Zhang, Y. Y. Li, Y. X. Jiang, S. G. *Sun, Journal of Electrochemistry*, 2014, 20, 395-400.

[16] a) V. Del Colle, J. Souza-Garcia, G. Tremiliosi-Filho, E. Herrero, J. M. Feliu, *Physical chemistry chemical physics* **2011,** *13*, 12163-72; b) L. Jiang, L. Colmenares, Z. Jusys, G. Q. Sun, R. J. Behm, *Electrochim. Acta* **2007,** *53* (2), 377-389.

[17] W. Du, G. Yang, E. Wong, N. A. Deskins, A. I. Frenkel, D. Su, X. Teng, *J Am Chem Soc* **2014,** *136*, 10862-5.

[18] a) T. Sheng, W. F. Lin, C. Hardacre, P. Hu, Phys. Chem. Chem. Phys., **2014**, 16, 13248-13254; b) T. Sheng, W. F. Lin, S. G. Sun, Phys. Chem. Chem. Phys., **2016**, 18, 15501-15504.

2-D S nanosheets were successfully in-situ grew on Cu foam current collector. When applied as cathode for room room-temperature Na-S batteries, the S cathode delivers ultrahigh electroactivity with the highest initial discharge/charge capacity of 3189/1403 mAh g^{-1}, which shows great potential to realize high-capacity S cathode.